

Forced Detachment of the CD2-CD58 Complex

M. V. Bayas,* K. Schulten,*† and D. Leckband*‡

*Center for Biophysics and Computational Biology; †Department of Physics; and ‡Department of Chemical and Biomolecular Engineering, University of Illinois at Urbana-Champaign, Champaign, Illinois 61801

ABSTRACT The force-induced detachment of the adhesion protein complex CD2-CD58 was studied by steered molecular dynamics simulations. The forced detachment of CD2 and CD58 shows that the system can respond to an external force by two mechanisms, which depend on the loading rate. At the rapid loading rates of 70 and 35 pN/ps (pulling speeds of 1 and 0.5 Å/ps) the two proteins unfold before they separate, whereas at slower loading rates of 7 and 3.5 pN/ps (pulling speeds of 0.1 and 0.05 Å/ps), the proteins separate before the domains can unfold. When subjected to a constant force of 400 pN, the two proteins separated without significant structural distortion. These findings suggest that protein unfolding is not coupled to the adhesive function of CD2 and CD58. The simulations further confirm that salt bridges primarily determine the tensile strength of the protein-to-protein bond, and that the order of salt bridge rupture depends mainly on the position of the bond, relative to the line of action of the applied force. Salt bridges close to this line break first. The importance of each of the salt bridges for adhesion, determined from the simulations, correlates closely with their role in cell-to-cell adhesion and equilibrium binding determined by site-directed mutagenesis experiments.

INTRODUCTION

Cell surface proteins mediate intercellular recognition and adhesion. In the immune response, a host of proteins is involved in the recognition of antigen presenting cells by T-cells. These include the T-lymphocyte adhesion receptor CD2 and its ligands (Davis et al., 1998a). Ligand binding by CD2 has several distinctive characteristics. The bonds have low affinity (μM) (Davis et al., 1998a,b), which is a consequence of fast off rates ($k_{\text{off}} > 1 \text{ s}^{-1}$) (Davis et al., 1998a). Additionally, the binding specificity is determined by charge complementarity, rather than by shape complementarity, between the contact surfaces (Davis et al., 1998a; Arulanandam et al., 1993, 1994; Wang et al., 1999; Ikemizu et al., 1999).

Specifically, the interaction between CD2 and its ligand CD58 (LFA-3) is believed to augment the adhesion between the T-cell and antigen presenting cells (Davis et al., 1998a; Moigneon et al., 1989). This in turn enhances antigen recognition in vitro (Moigneon et al., 1989; Koyasu et al., 1990). Both CD2 and CD58 are immunoglobulin superfamily proteins, and their ectodomains consist of two tandemly arranged Ig-type domains (Bodian et al., 1994; Ikemizu et al., 1999), in which adhesion is mediated by their membrane distal N-terminal-domains (D1) (Arulanandam et al., 1993; Wang et al., 1999; Moigneon et al., 1989; Koyasu et al., 1990; see also Fig. 1 *a*).

The adhesive domains of both proteins have a V-set topology composed of nine β -strands distributed in two sheets. Unlike canonical V-set structures there is no disulfide bond between strands *B* and *F* (Wang et al., 1999; Bodian et al., 1994; Ikemizu et al., 1999; Bork et al., 1994; Chothia

and Jones, 1997; see also Fig. 1 *b*). Experimental evidence, including equilibrium binding and mutagenesis studies, shows that the contact area involves mainly the C, C' and C'' β -strands and the FG, CC', and C'C'' loops of these domains (Davis et al., 1998a,b; Wang et al., 1999; Ikemizu et al., 1999). Most of the residues in these regions are charged, and the only three hydrophobic residues situated at the interface are F46 and P80 of CD58 and Y86 of CD2. The charged residues at the adhesive interface form the following interprotein salt bridges (CD2 residue given first): D32K34, D31R44, K34E78, K41D84, K43E25, R48E37, R48E39, K51E42, K51E39, and E95K32 (Wang et al., 1999) (compare with Fig 1, *d-f*). The locations of the different residues are listed in Table 1.

Early studies tested the involvement of these charged residues in protein recognition and cell adhesion (Arulanandam et al., 1993, 1994). These authors evaluated the effect of point mutations on cell-to-cell adhesion. For CD2, the alanine point mutations K41A and E95A had the weakest effect, reducing cell-to-cell adhesion to 56% and 86% of wtCD2, respectively. The mutations K34A, K43A, and K51A had a stronger effect, reducing the adhesion to less than 15% of the wild-type value. The mutations D32A, R48A, and K91A abolished adhesion completely (Arulanandam et al., 1993). In the case of CD58, the alanine point mutations E39A, E78A, and D84A had no effect. Mutations E25A, K32A, and R44A had a modest effect, reducing the adhesion to between 40% and 86% of that of wtCD58. Mutations D33A, K34A, and E37A had the strongest effect, reducing binding to less than 30% (Arulanandam et al., 1994). The authors of these studies established that the mutations had no effect on the three-dimensional structure of the adhesion domains (Arulanandam et al., 1993, 1994).

A comparison of the mutagenesis results with the salt bridge pairings listed in Table 1 reveals the role of some of the polar residues. Of the six point mutations with the

Submitted July 21, 2002, and accepted for publication December 5, 2002.

Address reprint requests to D. Leckband, 114 Roger Adams Laboratory, University of Illinois at Urbana-Champaign, Box C-3, 600 S. Mathews Ave., Urbana, IL 61801. Tel.: 217-244-0793; Fax: 217-333-5052; E-mail: leckband@uiuc.edu.

© 2003 by the Biophysical Society

0006-3495/03/04/2223/11 \$2.00

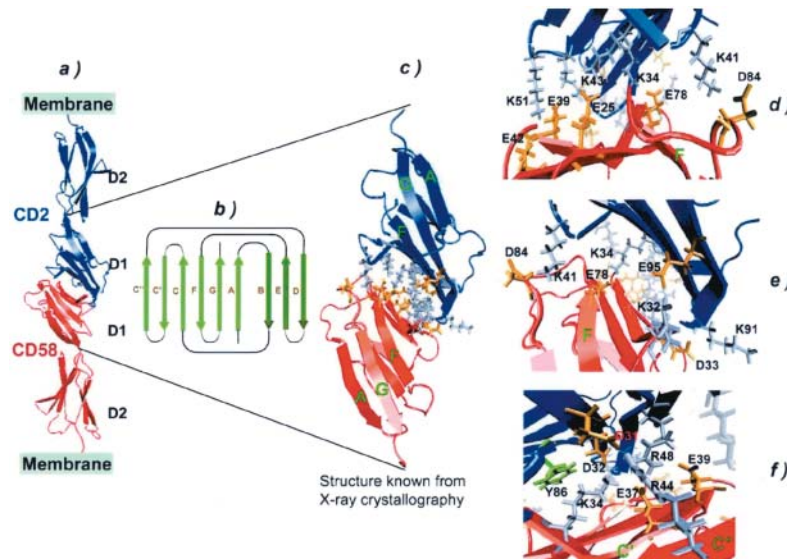


FIGURE 1 (a) Predicted structure of the adhesive CD2-CD58 complex. The Brookhaven Protein Data Bank entries 1HNF (Bodian et al., 1994) and 1CCZ (Ikemizu et al., 1999) were used to prepare the representations of CD2 and CD58 respectively. (b) Topology of the binding domains of CD2 and CD58. (c) Representation of the adhesive complex involving domains D1. This corresponds to the entry 1QA9 (Wang et al., 1999), with most of the charge amino acids in the binding interface in bond representation. All of the charged residues, except K91 and D33, form salt bridges. The different salt bridges are shown from the front (d), the left (e), and from the back (f). Several amino acids in the binding interface form multiple contacts. This is the case of CD2 K51, which forms salt bridges with CD58 E39 and CD58 E42 (d). CD2 R48 similarly forms salt bridges with CD58 E37 and CD58 E39 (f).

strongest effect—that is, D32A, R48A, K91A of CD2 and D33A, K34A, and E37A of CD58—four involve residues forming part of the observed salt bridges, namely D32K34 and R48E37. Actually, the D32K34 salt bridge is directly involved in a region identified as the energetic *hot spot* of the CD2-CD58 interaction (Kim et al., 2001). The pair K91-D33 is special because, although it appears to be as important as D32-K34 and R48-E37, the side groups do not form a salt bridge, despite their close proximity (Wang et al., 1999). The question arises as to whether conformational fluctuations permit these side chains to form a salt bridge, and thereby explain the strong effect of the two respective point mutations. One may expect that the mentioned side groups form salt bridges en route during complex formation or detachment. On the other hand, the salt bridges K41D84 and E95K32 do not seem to be important for complex

formation and stability inasmuch as alanine mutations had weak or no effects.

Not all of the mutagenesis results permit one to draw conclusions about the functional importance of the salt bridges in the CD2-CD58 interface. For example, in the case of the salt bridge K51-E39, mutation K51A had a strong effect whereas E39A had no effect. This is reasonable if we consider that the elimination of K51 means the elimination of two salt bridges (K51E39 and K51E42) whereas the elimination of E39 does not necessarily prevent the formation of the K51E42 salt bridge. This particular point is suggested by Fig. 1 d. Likewise, there are no conclusive functionality roles for salt bridges D31R44, K34E78, and K43E25.

Charged residues in the interfacial region are not the only amino acids important for the complex stability. Recently, a calorimetry study quantified the impact of CD2 mutations on the binding affinity (Kim et al., 2001). According to this study the CD2 mutant Y86A reduced the affinity for CD58 ~1000-fold whereas the mutants D31A, D32A, K34A, K43A and R48A reduced the affinity by only 47 to 127-fold. In the crystal structure of the CD2-CD58 complex, the aromatic ring of Y86 packs against the aliphatic chain of K34 of CD58 (see Fig. 1 f; see also Wang et al., 1999). Nevertheless, while the importance of these residues in equilibrium binding is now well established, their role in adhesion has not been determined.

Within this context, two issues are of particular interest with respect to the adhesive function of CD2 and CD58. First, the mutagenesis studies mentioned above identified the functional roles of some of the amino acids in CD2:CD58 binding. However, their role in bond stabilization and rupture are unknown. Earlier studies (Chilkoti et al., 1995) suggested that side chains that contributed to the streptavidin-biotin binding affinity did not necessarily have an an-

TABLE 1 Charged residues forming salt bridges at the CD2/CD58 interface

CD2		CD58	
Residue	Localization	Residue	Localization
D31	C	R44	C''
D32	C	K34	CC'
K34	C	E78	F
<u>K41</u>	<u>CC'</u>	<u>D84</u>	<u>FG</u>
<u>K43</u>	<u>CC'</u>	<u>E25</u>	<u>C</u>
R48	C'C''	E37	C'
R48	C'C''	E39	C'C''
K51	C'C''	E39, E42	C'C''
<u>E95</u>	<u>G</u>	<u>K32</u>	<u>CC'</u>

The residues in the same row belong to the same salt bridge. The boldface rows correspond to the salt bridges that are the most important for adhesion. The underlined rows correspond to the less important ones. The plainface rows indicate that the importance of the correspondent salt bridges is uncertain. The localization entries refer to either b-strands (single letter) or loops (two letters) of the proteins according to the notation shown in Fig. 1 b.

alogous impact on the adhesion strength. The same may apply for the CD2-CD58 interaction. Second, other Ig-type domains unfold under force (Marszalek et al., 1999; Lu et al., 1998). It has been proposed that the forced unfolding of domains in cell adhesion molecules modulates their adhesive properties (Carl et al., 2001; Fisher et al., 2000).

Steered molecular dynamics (SMD) simulations are particularly suited to address these issues. SMD simulations have been used in numerous studies of the mechanisms of force-induced bond failure (Izrailev et al., 1997; Lu et al., 1998; Isralewitz et al., 2001). With this approach, an external force applied to the system of interest can induce ligand unbinding and/or conformational changes on time scales accessible to molecular dynamic simulations (Izrailev et al., 1997; Lu et al., 1998; Isralewitz et al., 2001). Such investigations reveal the atomic level details of the complex as the molecules are pulled apart. Although the timescales are much faster than in typical experiments, this approach has generated several predictions that were subsequently verified by experiment (Marszalek et al., 1999; Lu et al., 1998; Krammer et al., 1999). They have also explained experimental observations (Evans and Ritchie, 1997). In this report, we used SMD simulations to investigate the detachment of the N-terminal domains of CD2 and CD58. These results not only confirmed previous experimental findings, but also revealed the molecular details underlying the complex detachment. They further demonstrated that, although the individual domains unravel at ultrafast pulling rates, much slower pulling speeds result in preferential bond rupture and little domain distortion.

METHODS

The steered molecular dynamic simulations were performed under both constant pulling velocity (cv-SMD) and constant force (cf-SMD) with two sets of conditions using the program NAMD (Kale et al., 1999) and the CHARMM22 force field (MacKerell et al., 1998). The visualization, molecular graphics, and analyses of the simulations were performed using the program VMD (Humphrey et al., 1996). The crystal structure of the CD2-CD58 complex (Wang et al., 1999) deposited in the Brookhaven Protein Data Bank as entry 1QA9 was used as the starting point. We first transformed the original coordinate system of the complex to one where the z -axis is along the line joining the backbone C carbons of CD2-R105 and CD58-S95. The force was applied along the z -axis.

In a first set of conditions, which we will call SET 1, the complex was solvated in a box of explicit water molecules with dimensions $79.8 \times 84.9 \times 161.1 \text{ \AA}^3$. The solvation was performed using the “solvate” feature of the package VMD (Humphrey et al., 1996). Three Cl^- ions and seven Na^+ ions were added to the system, keeping the system neutral. The final system contained 104,000 atoms 3228 of which belong to the complex. The large ratio of solvent to protein atoms is due to the elongated form of the water bath chosen to permit separation of the complex.

SET 1 simulations were performed with a time step of 1 femtosecond, a uniform dielectric constant of 1, periodic boundary conditions, and a cutoff of nonbonded forces with a switching function starting at a distance of 8 \AA and reaching zero at 12 \AA . The energy of the system was initially minimized in two stages. First, the coordinates of the complex were kept fixed for 10,000 steps of minimization. Then, allowing the movement of the complex, except for the backbone C atoms of CD2-R105 and CD58-S95, the system

was minimized again for another 10,000 steps. The minimization was performed at 0 K followed by heating the system to 298 K in 20,000 steps. During the heating, the two atoms mentioned previously remained fixed.

Finally, the system was equilibrated at 298 K and 1 atm for 1.5 ns. The temperature was controlled using Langevin dynamics, and the pressure was controlled using the Langevin piston pressure control. During the first ns of the equilibration the restraints were decreased but the backbone C atoms of CD2-R105 and CD58-S95 were still held fixed. After that, the system was allowed to evolve for 0.5 ns keeping the backbone C atom of CD58-S95 fixed and the backbone C atom of CD2-R105 restrained to move freely only in the z direction. Fig. 2 *a* shows the evolution of the backbone root mean-squares deviation (RMSD) of the system during equilibration. The RMSD during the last 0.3 ns was 1.057 ± 0.077 . The size of the water box at the end of the equilibration was $81.6 \times 80.1 \times 152.8 \text{ \AA}^3$. The state at 1.5 ns was used as the initial one for the first set of cv-SMD simulations.

We used SET 1 conditions for simulations at constant pulling velocity (cv-SMD). In this case, the backbone C atom of CD58-S95 was fixed whereas an external force along the z -axis was applied to the backbone C atom of CD2-R105. The external force had the form:

$$F = k(vt - \Delta z).$$

Here Δz is the z -displacement of the pulled atom relative to its original position, v is the velocity of one end of a harmonic spring if it were attached to the pulled atom by the other end (Lu et al., 1998), and k is the spring constant. The simulations were performed with a spring constant of $1 k_B T/\text{\AA}^2$ ($\sim 70 \text{ pN/\AA}$) and four pulling speeds: 1, 0.5, 0.1, and 0.05 $\text{\AA}/\text{ps}$. For each velocity, the time evolution of the force (F), the z displacement of the pulled atom (Δz), and the relative z displacement of the centers of mass of CD2 and CD58 were monitored. It is important to mention that Δz is also the increment of the end-to-end distance of the complex in the direction of the applied force. In the following, Δz will be referred as the “extension” and the relative z -displacement of the centers of mass will be referred as the “separation.”

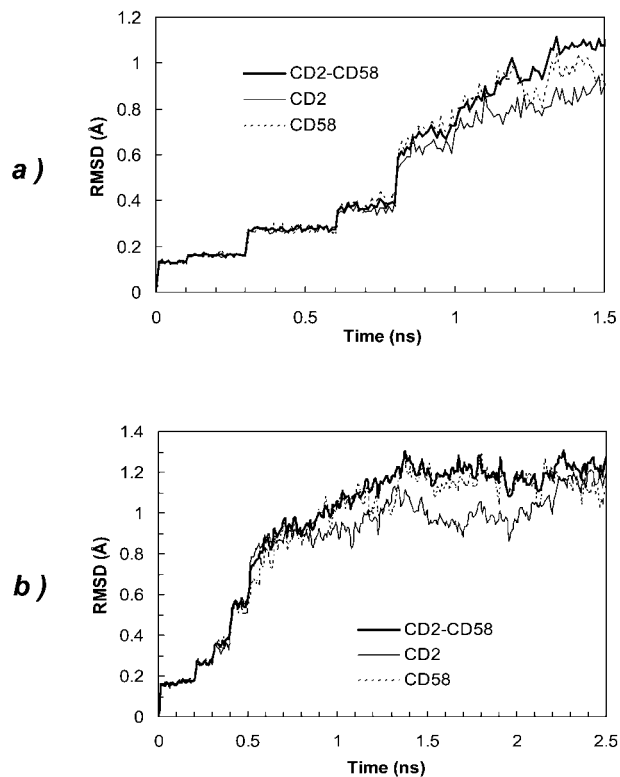


FIGURE 2 Evolution of the backbone RMSD as a function of time during the equilibration process, for SET 1 (*a*) and SET 2 (*b*) set of conditions.

A second set of simulations, SET 2, used a smaller water box, different parameters for the switching function for long-range interactions, and full electrostatics. The other modeling conditions were the same as in SET 1. The box of explicit water molecules had dimensions $79.8 \times 84.9 \times 141.1 \text{ \AA}^3$. The final system contained 90,916 atoms, 3228 of which belong to the complex. For the nonbonded forces, we used a switching function starting at a distance of 10 \AA and reaching zero at 14 \AA . The full electrostatic calculations were performed using the Particle Mesh Ewald method implemented in the NAMD package (Kale et al., 1999). The purpose of this was to make sure that the results found in the first set of simulations were not undermined by incomplete electrostatics. The consistency between the simulations showed that this is not the case.

The minimization and heating of the system were as in SET 1, except that the equilibration lasted 2.5 ns. During the first 0.5 ns the restraints were decreased but the backbone C atoms of CD2-R105 and CD58-S95 were still held fixed. After that, the system was allowed to evolve for 2 ns keeping the backbone C atom of CD58-S95 fixed and the backbone C atom of CD2-R105 restrained to move freely only in the z -direction. The purpose of this longer equilibration was to test the possibility of formation of a salt bridge between the CD2-residue, K91 and the CD58-residue, D33. The backbone RMSD of the complex during the last 1 ns of the last phase of equilibration was 1.197 ± 0.045 . Fig. 2 *b* shows the evolution of the backbone RMSD. The size of the water box at the end of the equilibration was $73.2 \times 82.3 \times 144.2 \text{ \AA}^3$. The final state after 2.5 ns equilibration was used as the initial one for the second set of simulations. This included four cv-SMD simulations using the same spring constant at the same pulling speeds as before, and one simulation using constant force of 400 pN. The purpose of the latter simulation was to study the behavior of the system under conditions where thermal fluctuations had an extensive opportunity to contribute to bond rupture.

RESULTS

The cv-SMD simulations were performed using both sets of conditions SET1 and SET2. Because they yielded the same qualitative results, only the SET1 simulations will be described in detail. At pulling speeds of 1 and $0.5 \text{ \AA}/\text{ps}$ the complex extension was primarily due to partial unraveling of the proteins. The G -strands of both CD2 and CD58 unraveled and pulled their respective A -strands with them. Fig. 3 shows snapshots from the simulation performed at the pulling speed of $1 \text{ \AA}/\text{ps}$.

Fig. 4 *a* shows the evolution of the force and displacements for the pulling speed of $1 \text{ \AA}/\text{ps}$. The system was pulled for 120 ps. The final extension of the complex was 86 \AA , whereas the separation was 27 \AA . During the first 28 ps the force increased continuously at a rate of $48.5 \text{ pN}/\text{ps}$ and the system extended without rupture. At 28 ps (point *a*), the extension and separation were 8.45 and 0.62 \AA , respectively. From 28 ps to 67 ps the slope of the force decreased to $27.7 \text{ pN}/\text{ps}$, mainly due to the first rupture events. During this period the salt bridges close to the line of action of the force, namely K41D84, E95K32, and K34E78, broke. The separation of the G -strands of both CD58 and CD2 began in this period at 41 ps and 57 ps, respectively. At these times, the most external hydrogen bonds between the G - and F -strands of the proteins were broken. The remaining hydrogen bonds broke almost simultaneously at $\sim 67 \text{ ps}$ (point *b*) generating a plateau in the force profile. The plateau ended with the formation of new transitory H-bonds between the G - and F -strands of CD2 that broke around the maximum (point *c*)

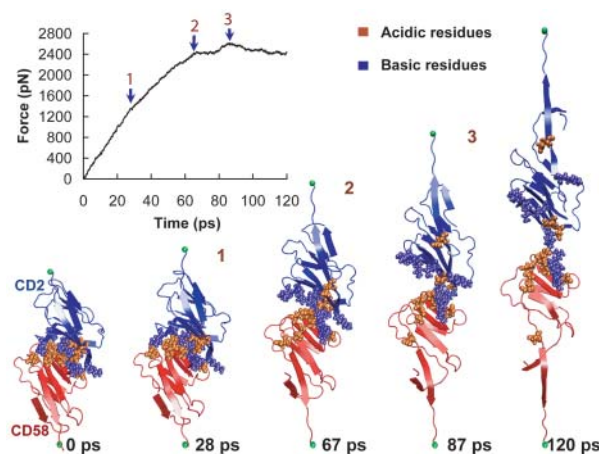


FIGURE 3 Snapshots of the complex during the simulation performed at $1 \text{ \AA}/\text{ps}$. The inset shows the corresponding force-extension profile. The charge residues in the binding region are highlighted using a VDW representation. The sequential rupture of the salt bridges and the partial unraveling of the proteins are visualized in these figures.

in the force profile. The G -strands separated completely after this. At 120 ps the G -strands of both proteins were completely unraveled, and only the salt bridges K51E39 and K51E42 remained. At this point, the backbone RMSD values of CD2 and CD58 measured 8.9 and 9.6 \AA , respectively.

Fig. 4 *b* shows the evolution of the force and the displacements for the pulling speed of $0.5 \text{ \AA}/\text{ps}$. The system was pulled for 210 ps, and the final extension of the complex was 88.2 \AA , whereas the final separation was 27.7 \AA . The degree of unraveling of CD2 was similar to the one obtained at $1 \text{ \AA}/\text{ps}$, but the degree of unraveling of CD58 increased. This is principally due to the additional rupture of the hydrogen bonds between the F and C strands. During the first 20 ps the force increased continuously at a rate of $20.4 \text{ pN}/\text{ps}$ without any rupture. At 20 ps (point *a*), the extension was 2.7 \AA and the separation was 0.19 \AA . From 20 ps to 75 ps, the first rupture events decreased the slope of the force to $16.2 \text{ pN}/\text{ps}$. During this period the K41D84 and K34E78 salt bridges broke. Additionally, at 51 ps the strand F of CD58 started to separate from strand C . However, these strands did not separate completely until 200 ps. At 75 ps (point *b*) the G -strand of CD58 began to separate, causing an additional change in the slope of the force profile. From 75 ps to 114 ps, the slope of the force profile decreased to $11.8 \text{ pN}/\text{ps}$. The separation of the G -strand of CD58 was complete at 114 ps (point *c*). The separation of strands F and G of CD2 started later at 128 ps, and was complete at 150 ps (point *d*). After this, the force decreased steadily as the proteins unraveled. At 210 ps, the G -strands of both proteins and the F -strand of CD58 were completely separated, and the only salt bridges remaining were D31R44, K51E39, and K51E42. At this point, the backbone RMSD values of CD2 and CD58 were 8.1 and 10.7 \AA , respectively.

At pulling speeds of 0.1 and $0.05 \text{ \AA}/\text{ps}$, the degree of unraveling of the proteins decreased substantially and the

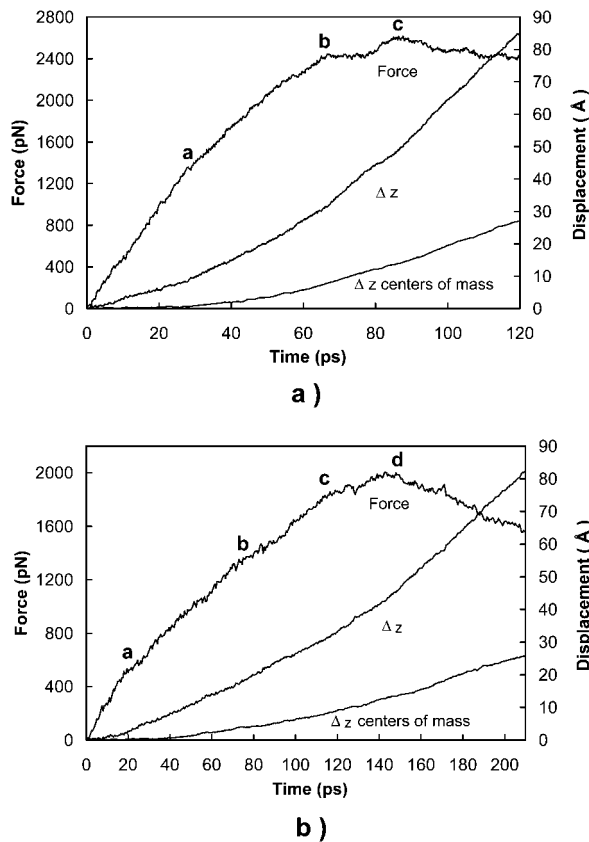


FIGURE 4 Force-extension profile and displacements at 1 Å/ps (a) and 0.5 Å/ps (b). In both cases the separation (Δz centers of mass) remains close to zero at the beginning, whereas the extension (Δz) increases rapidly. This is accompanied by a uniform increase of the force until point *a* in both figures. After this period the main rupture events occur. At point *b* in Fig. 4 *a*, strand *G* of CD2 separates. This generates a plateau in the force profile. At point *b* in Fig. 4 *b* strand *F* of CD58 partially separates from strand *C* and at point *c* strand *G* separates completely. For both pulling speeds the complete separation of strands *G* of CD2 and CD58 occurs around the maximum of the force (point *c* in Fig. 4 *a* and point *d* in Fig. 4 *b*). The difference between the extension and separation at the end of the simulations are due primarily to the protein unraveling.

rupture of the salt bridges determined the main features of the force profile. The force profile can be divided into three time periods. In period I, the force increased continuously and the salt bridges at the CD2-CD58 interface near the line of action of the force broke. In period II, the remaining contacts broke while the force remained relatively constant. In period III, the proteins were completely separated and slightly deformed compared with their original shape. Fig. 5 shows snapshots from the simulation performed at 0.05 Å/ps with the first set of conditions (SET 1).

Fig. 6 *a* shows the time evolution of the force and the displacements at a pulling speed of 0.1 Å/ps. In period I (0–336 ps), the average force increased at a rate of 3.12 pN/ps. During the first 150 ps, the extension of the complex did not yet lead to separation. The separation began only after the rupture of the K34E78 salt bridge at 222 ps. An important

event in period I was the formation of an additional salt bridge between CD2-K91 and CD58-D33 at 300 ps. This period ended with the rupture of the outermost hydrogen bond between strands *G* and *F* of CD58 that caused a decrease in force (point *a* in Fig. 6 *b*). At this moment the system was extended by 20 Å, but the separation was only 5 Å. During period II, the extension of the complex continued, in part, because of the partial separation of the *F*- and *G*-strands of CD58. However, the main cause for the extension in this region was the rupture of the remaining salt bridges. Fig. 6, *b–d* show the relationship between the main molecular rupture events and the features of the force profile. The salt bridge D31R44 was the last to break at 570 ps (point *f* in Fig. 6 *d*). At this point, the extension and separation were 42 Å and 18.4 Å, respectively. This is the beginning of period III. The simulation lasted 650 ps, after which CD2 had a backbone RMSD of 1.89 Å and that of CD58 was 3.25 Å.

Fig. 7 *a* shows the evolution of the force and the displacements for the pulling velocity of 0.05 Å/ps. In period I (0 to 648 ps), the average time increment of the force was 1.2 pN/ps, and the salt bridges K41D84, K34E78 and E95K32 broke. Surprisingly, the salt bridge K51E42 also broke during this period. Period I ended with the breaking of the D32K34 contact at 648 ps (point *a* in Fig. 7 *c*). At this point, the extension and separation were 21 Å and 6.4 Å, respectively. In period II, the extension of the complex was due to the breaking of the rest of the salt bridges and partly to the separation of the *F*- and *G*-strands of CD58 that occurred at 748 ps (point *b* in Fig. 7 *b*). Fig. 7, *b–d* show the relation between the main rupture events and the features of the force profile. The salt bridge D51E39 was the last to break, at 960 ps (point *d* in Fig. 7 *d*). At this moment, the extension and separation measured 39 Å and 18.2 Å, respectively. This is the beginning of period III. The simulation lasted 1000 ps. At this time, CD2 had a backbone RMSD of 1.93 Å and that of CD58 was 3.14 Å.

A comparison of the constant velocity simulations shows how the mechanism of elongation changes with the pulling speed. The simulations were compared by plotting the evolution of the force and extension as a function of the spring displacement (equal to $v t$, where v is the pulling speed). Fig. 8 *a* shows that, as the pulling speed decreases, the complex elongates more readily, and the force to extend the complex decreases (Fig. 8 *b*). Additionally, for speeds of 1 Å/ps and 0.5 Å/ps, there is significant unraveling of the proteins, and CD2 and CD58 do not separate in the time frame of the simulation. The force peaks preceding the complete unraveling of the *G*-strand of CD2 were ~2600 pN for 1 Å/ps and ~2000 pN for 0.5 Å/ps. These values are of the same order of magnitude as the force necessary to initiate the unfolding of the Ig domains of titin under the same conditions (Lu et al., 1998). This is consistent with the similarity between the structures of these proteins. The situation is different at speeds of 0.1 and 0.05 Å/ps. The proteins

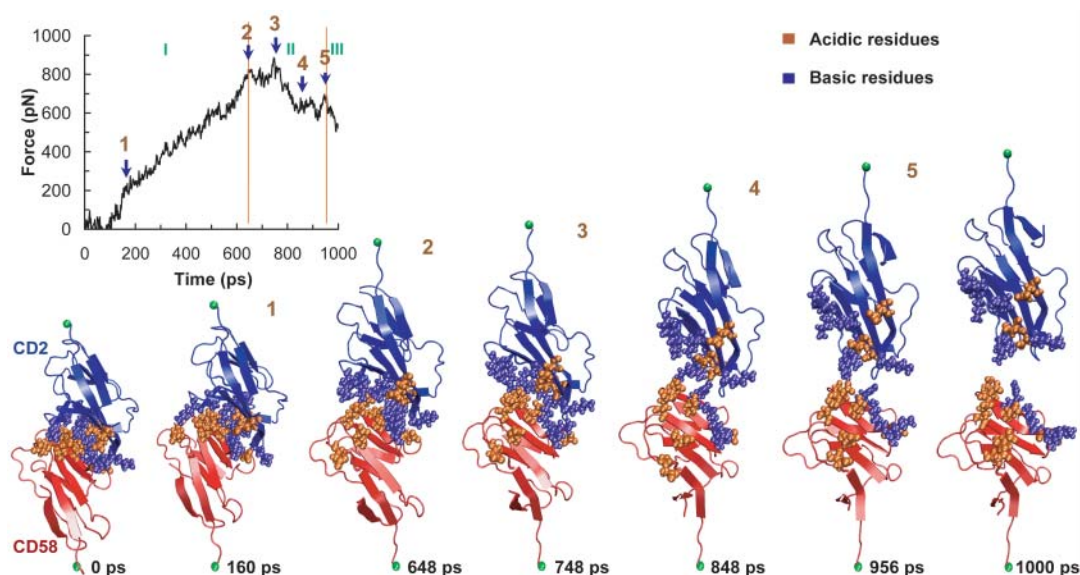


FIGURE 5 Snapshots and force-extension profile from the simulation at 0.05 \AA/ps . The charged residues in the binding region are highlighted using a VDW representation. The structures show the sequential breaking of the salt bridges that lead to the detachment of the complex. After detachment the protein structures are only slightly deformed.

do not unravel, and protein separation occurs at a small increase in the end-to-end distance of the complex following the sequential rupture of the salt bridges. Tables 2 and 3 summarize the different moments at which the salt bridges rupture.

An interesting feature observed in some of the simulations is the formation of a salt bridge between CD2-K91 and CD58-D33. As mentioned before, there is no salt bridge between those side chains in the crystal structure (Wang et al., 1999). Fig. 9 shows the formation and rupture of this salt bridge at the simulated pulling speed of 0.1 \AA/ps , using the first set of conditions. It formed at 300 ps and remained intact for a significant amount of time. The complex finally ruptured at 522 ps, and this salt bridge broke at 512 ps. For the simulations at 0.05 \AA/ps , this event was observed only during the simulation performed with the second set of conditions. It was also observed during the simulation at constant force. The important point is that the simulations show that the formation of a transient salt bridge between these residues is possible. This observation would account for the importance of these two residues for cell adhesion determined by mutagenesis (Arulanandam et al., 1993).

Fig. 10 shows the behavior of the system when it was pulled with a constant force of 400 pN. The sequential rupture of salt bridges is more evident in this simulation. The evolution of the separation shows the different steps leading to detachment. The transition to Plateau 1 involves the increment in the separation without rupture of any of the salt bridges. The salt bridge K91D33 was formed at this point. Plateau 2 was reached after rupture of the K41D84 and K34E78 salt bridges. A partial deformation of CD2 leads to Plateau 3 whereas a partial deformation of CD58 leads to

Plateau 4. Plateau 5 was reached after rupture of the K43E25 salt bridge. Upon the rupture of the D32K34 and R48E37 contacts, the system jumped to Plateau 6 which persisted until the K91D33 salt bridge broke. The rupture of the D31R44 and D51E39 salt bridges at 0.75 ns completed the detachment. The simulation lasted 0.8 ns. At this time, the proteins were only slightly deformed. CD2 had a backbone RMSD of 1.707 \AA and that of CD58 was 1.973 \AA .

In addition to the salt bridges, we also considered the hydrogen bond and van der Waals contacts that are mostly clustered around the region defined by the CD2-FG and the CD58-CC' loops (FGCC'). Of the five hydrogen bonds reported in the crystal structure, only two remained intact after the equilibration: namely, Asn92(HN)-Asp33(O1) and Gly90(O)-Lys34(HN) (CD2 residue given first). Close to these hydrogen bonds are two van der Waals contacts involving two of three hydrophobic amino acids present in the contact region: CD2-Tyr86 and CD58-Phe46. The aromatic ring of CD2-Tyr86 packs with the aliphatic part of CD58-Lys34 and the $C\alpha$ of CD2-Gly90 contacts CD58-Phe46. All of the contacts in the FGCC' region except Asn92(HN) - Asp33(O1) jumped apart around the same time as the salt bridge D32K34 broke, i.e., at 450 ps for 0.1 \AA/ps and at 650 ps for 0.05 \AA/ps . This behavior was observed in the rest of the simulations as well. The hydrogen bond Asn92(HN)-Asp33(O1) broke around the same time as the salt bridge E95K32, in all cases.

DISCUSSION

Our simulations show that two mechanisms characterize the response of the CD2-CD58 complex to an external force.

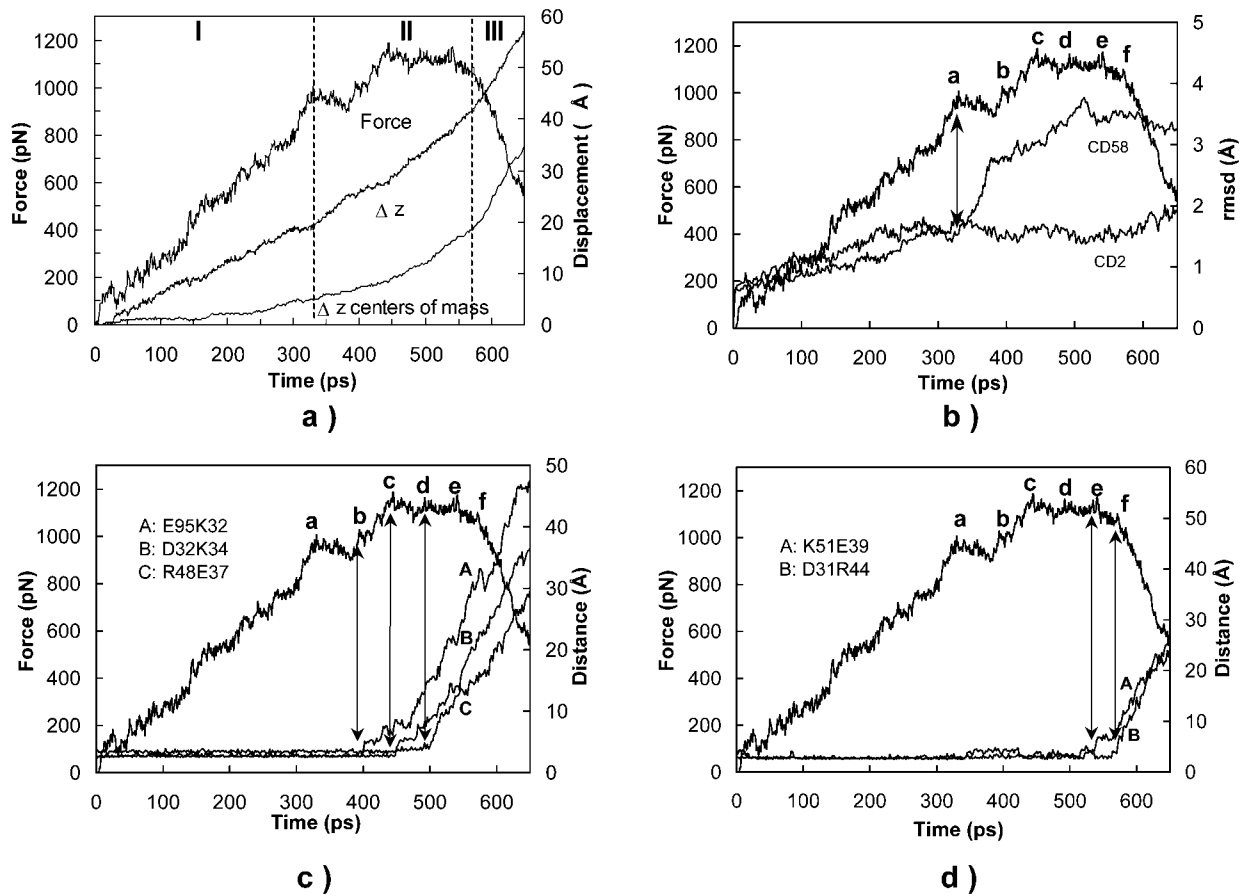


FIGURE 6 (a) Force-extension profile and displacements determined at 0.1 \AA/ps . (b) Variation of the RMSDs of the protein backbones versus time. At point *a*, the force decreases due to the partial separation of the *G* strand of CD58. CD2 did not rupture. (c) Distance between salt bridge pairs versus time. The rupture of the salt bridges E95K32, D32K34, and R48E37 are associated with the peaks at points *b*, *c*, and *d*, respectively. (d) Distance between salt bridge pairs versus time. At points *e* and *f*, salt bridges K51E39 and D31R44 broke.

The first is linked to the structural integrity of the proteins, and dominates at high loading rates. The second mechanism involves the rupture of the binding contacts, and is the predominant mechanism at low loading rates. This scenario is consistent with the notion that the relative strengths of single bonds depend on the loading rate (Evans and Ritchie, 1997; Evans, 1998). In the case of the CD2-CD58 complex, the bonds stabilizing the domain structure and those stabilizing the protein-to-protein interface are in series. Depending on the activation energies and positions of the transitions states for the two mechanisms, the preferred response to force can switch when the system is pulled at a different rate (Evans, 1998). Thus, the loading conditions used will determine whether bond rupture precedes protein deformation or vice versa. In our simulations, the crossover to preferential CD2-CD58 bond rupture occurred at the slower loading rates. Provided that there is only one crossover between the two mechanisms, one can reasonably extrapolate these observations to the much slower loading rates of either force probe measurements or the rates encountered *in vivo*. This suggests that protein unfolding is not cou-

pled to the adhesive function of these proteins. This is supported experimentally by direct force measurements of the interaction between the rat analogs rCD2 and rCD48. In those measurements, the complex failed at an end-to-end distance commensurate with rupture at the protein-to-protein interface (Zhu et al., 2002).

The results of the cf-SMD simulation further support this conclusion. This simulation showed that pulling the system with a force lower than that needed to unfold the domains in the cv-SMD simulations only results in protein-to-protein detachment. The constant force also counters the argument that the short time scales of the SMD simulations bias the results by excluding the effects of fluctuations.

Although, the time scales of MD simulations are several orders-of-magnitude shorter than those of typical experiments, it has been demonstrated that the SMD results and experiments are not disconnected (Evans and Ritchie, 1997). In a few notable cases, the molecular details revealed in the simulations were shown to govern or predict experimentally measured behavior (Evans and Ritchie, 1997; Lu et al., 1998; Marszalek et al., 1999; Krammer et al., 1999). Clearly the

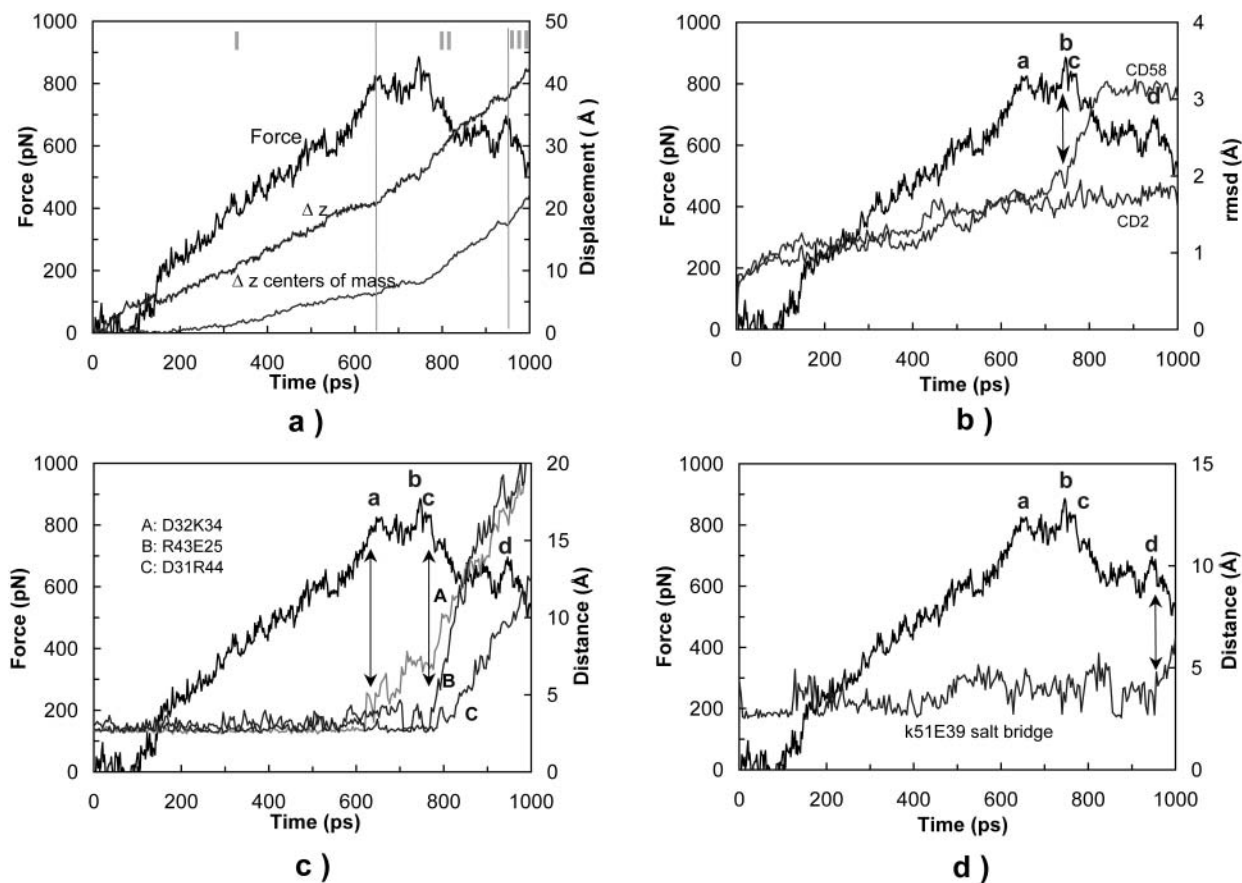


FIGURE 7 (a) Force-extension profile and displacements for 0.05 Å/ps. (b) Variation of the backbone RMSD of the proteins versus time. At point *b* the partial separation of the *G*-strand of CD58 caused a peak in the force profile. CD2 did not exhibit any abrupt rupture. (c) Distance between salt bridge pairs versus time. The rupture of the salt bridge D32K34 caused the force peak observed in point *a*. At point *c* the salt bridges E43E25 and D31K44 broke. (d) Distance between salt bridge pairs versus time. At point *d*, the salt bridge K51E39 broke, after which the proteins separated quickly.

values of the forces or times scales cannot be compared directly with experiments, but linking the molecular interactions revealed by the simulations to *in vivo* behavior is justified.

In this study, the simulations reveal that the interprotein salt bridges determine not only the binding specificity but also the tensile strength of the complex. In most of the cases, the sequence in which the salt bridge ruptures parallels their importance in cell-to-cell adhesion (Arulanandam et al., 1993, 1994). Mutagenesis studies showed that mutations at CD2-K41 and CD58-E95 do not completely eliminate adhesion. The simulations show that, while the salt bridges involving these residues break first, this bond failure does not have a major effect on the strength of the adhesive complex. On the other hand, the experiments showed that mutations of CD2-residues D32 and R48 completely abrogate adhesion (Arulanandam et al., 1993). In the simulations, the salt bridges involving the latter residues break in the second half of the detachment period in all of the simulations. Additionally, in the cv-SMD simulations, they contribute significantly to the force required to induce the final complex failure. There is therefore a close correlation between the

effect of the side chains on the bond strength and their influence on both the binding affinity and experimentally measured cell-to-cell adhesion. Because of the contribution of other residues to both the time of detachment and unbinding force (the latter only for cv-SMD), the simulations suggest that a single mutation in such residues as D32, R48, or K91 might increase the rate of complex rupture, but would not abolish adhesion altogether. However, no adhesion was observed with either of these mutants (Arulanandam et al., 1993). This could be a consequence of very fast dissociation rates. It could also indicate that these residues play an important role in molecular association, which was not probed in the adhesion study.

Our simulations also revealed that geometry, rather than differences in the relative strengths of the salt bridges, determines the sequence of salt bridge failure. Each of the single salt bridges should have comparable intrinsic binding energies. However, the bonds close to the line of force (e.g., K41D84) are the first to develop significant tension, and thus break first. As the initial bonds break, those far away initially resist the strain, and rupture later. The fact that the salt bridge K51E42 breaks early in the SET 1 simulation at 0.05 Å/ps,

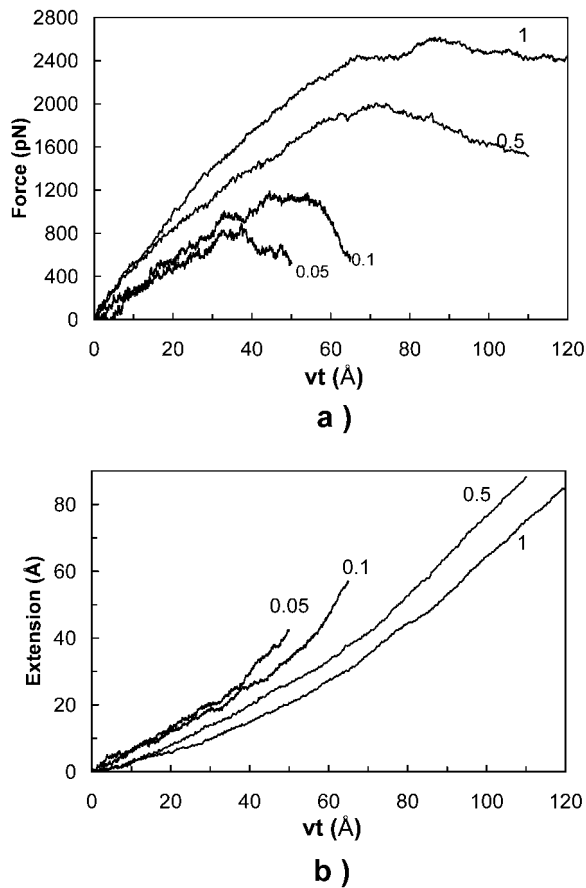


FIGURE 8 Force (a) and extension (b) as a function of the spring displacement determined at the four pulling speeds for the SET 1 conditions.

although it is somewhat far away, reveals that it is less stable than the others. This could be due to solvent exposure. Moreover, the rupture of this contact can be interpreted as a random event in the same way as the formation of the salt bridge K91D33 can. The dynamics of the formation and rupture of contacts during detachment may be an intrinsic part of the complex stability. Additionally, the degree of

TABLE 2 Rupture times of the salt bridges at pulling speeds 1 and 0.5 Å/ps

	1 Å/ps			0.5 Å/ps		
	Time (ps)	v t (Å)	Separation (Å)	Time (ps)	v t (Å)	Separation (Å)
K41D84	40	40	14.88	40	20	0.56
K34E78	47	47	18.22	51	25.5	1.39
E95K32	44	44	17.553	81	40.5	4.31
K43E25	65	65	30.109	117	58.5	8.48
D32K34	80.5	80.5	44.76	173	86.5	18.76
R48E37	88	88	50.92	200	100	24.184
R48E39	103	103	67.36	200	100	24.184
K51E39	—	—	—	—	—	—
K51E42	—	—	—	—	—	—
D31R44	105	105	68.96	—	—	—

TABLE 3 Rupture times of the salt bridges at pulling speeds 0.1 and 0.05 Å/ps

	0.1 Å/ps			0.05 Å/ps		
	Time (ps)	v t (Å)	Separation (Å)	Time (ps)	v t (Å)	Separation (Å)
K41D84	280	28	3.7	204	10.2	0.4
K34E78	222	22.2	2.02	320	16	1.3
E95K32	400	40	7.15	344	17.2	2.1
K43E25	382	38.2	6.53	772	38.6	8.8
D32K34	450	45	9.05	648	32.4	6.1
R48E37	492	49.2	11.42	784	39.2	9.2
R48E39	508	50.8	12.33	516	25.8	4.6
K51E39	522	52.2	14.77	956	47.8	17.9
K51E42	526	52.6	14.71	160	8	0
D31R44	572	57.2	19.02	828	41.4	12.6

alignment also influences the time of rupture. In the case of E95K32 and K91D33 (when it is formed), the E95K32 bond is more aligned to the force and breaks first. This occurs despite the close proximity of the two bonds.

The hydrogen bonds and van der Waals contacts clustered in the FGCC' region (Wang et al., 1999), including the hot spot do not contribute much to the force-extension profiles at the loading rates used in this study. The cluster ruptures more rapidly than the longer-lived salt bridges, and almost simultaneously with the D32K34 salt bridge. Consequently, under conditions of force-induced detachment, the hot spot is equivalent to the salt bridges. This region of the binding site has the greatest influence on the binding kinetics of the CD2-CD58 complex but does not have the same impact on adhesion.

It has been proposed that the low affinity interactions between CD2 and its ligands facilitate efficient antigen recognition by providing highly dynamic contacts between T-cells and antigen-presenting cells. This may allow the sampling of peptide-MHC complexes within the contact region (Davis et al., 1998). As the cells migrate, the protein bonds will be under tension, so that the force exerted on the CD2-CD58 complex is analogous to the force applied in the simu-

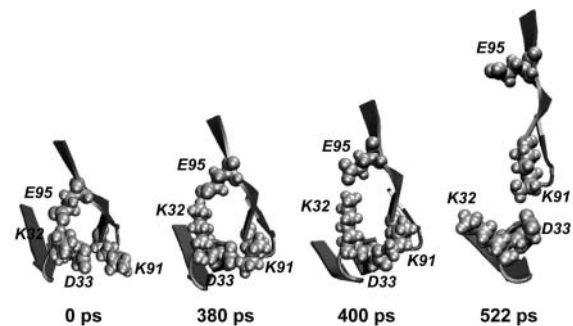


FIGURE 9 Snapshots showing the formation and rupture of the salt bridge K91D33 in the FGCC' region when the pulling speed was 0.1 Å/ps. The salt bridge formed at 300 ps. The neighboring salt bridge, E95K32, broke at 400 ps. The separation of the CD2-FC loop from the CD58-CC' loop was possible after the rupture of this salt bridge at 522 ps.

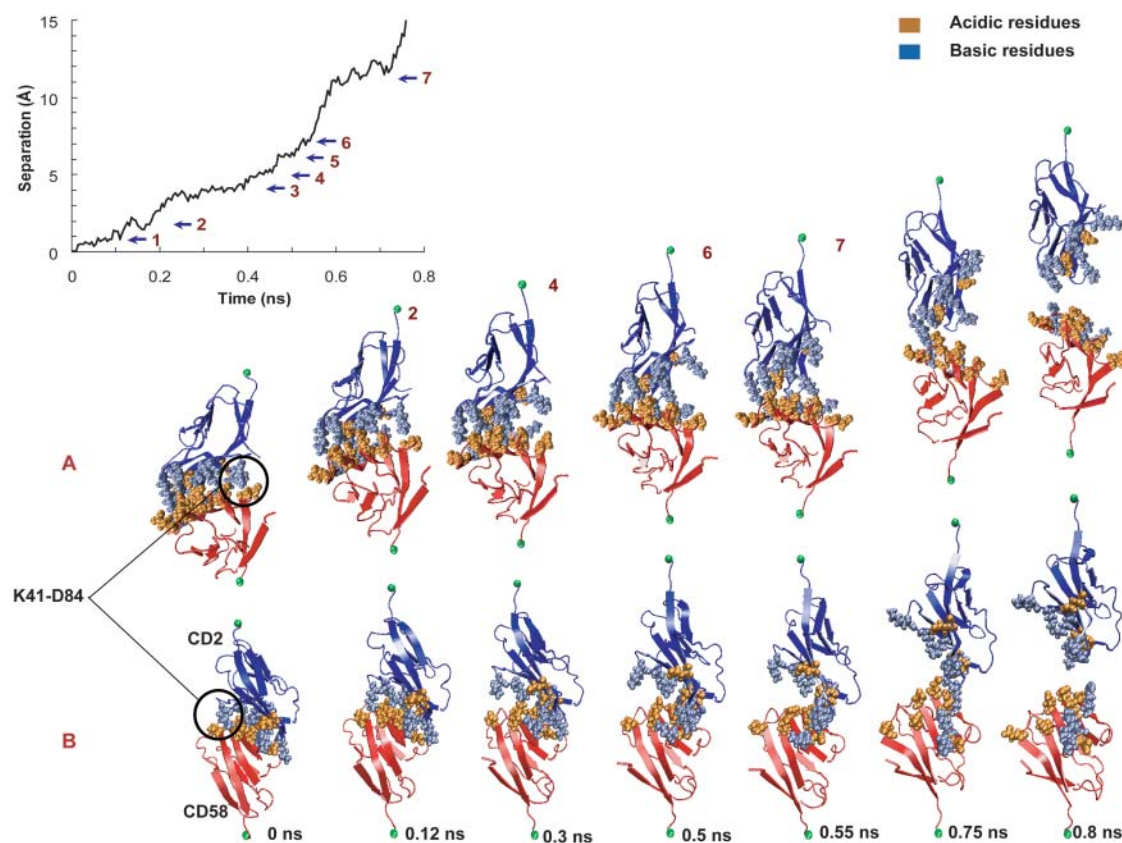


FIGURE 10 Snapshots and separation profile determined from the simulation at a constant force of 400 pN. In this case, the detachment occurred in seven steps; most of them involved ruptures of single salt bridges. The snapshots show the sequential breakage of the salt bridges leading to the detachment of the complex. *A* and *B* provide views of the CD2 and CD58 complex from two different angles. Charged residues in the binding region are highlighted using a VDW representation.

lations. Therefore, forced detachment *in vivo* is likely governed by the same interactions that these simulations identified as important.

In summary, the SMD simulations presented above provide molecular level insight into the mechanism of the adhesive failure of the CD2-CD58 complex. Although substantial protein deformations can occur under extremely rapid loading, the rate-dependent behavior suggests that, for this system, binding and unfolding are not coupled at much slower experimental and physiological loading rates. Furthermore, the tensile strength of the heterologous protein complex is governed by the same salt bridges that determine the proteins' binding affinity. Importantly, the simulations reveal how the sequential rupture (and formation) of these key salt bridges during detachment governs the strength of the CD2-CD58 complex. The simulations further identified key load-bearing amino acids that govern the tensile strength of this complex.

This work was supported by National Institutes of Health grants 1R01GM51338(DL), PHS5P41RR05969 (KS), and 1R01GM60946 (KS), and the National Science Foundation supercomputer time grant NRAC MCA93S028. M. Bayas was partially supported by the Ecuadorian Foundation for Science and Technology (FUNDACYT) and the "Escuela Politécnica Nacional" of Ecuador.

REFERENCES

- Arulananandam, A. R. N., J. M. Withka, D. F. Wyss, G. Wagner, A. Kister, P. Pallai, M. A. Recny, and E. L. Reinherz. 1993. The CD58 (LFA-3) binding site is a localized and highly charged surface area on the AGFCC' C' face of the human CD2 adhesion domain. *Proc. Natl. Acad. Sci. USA.* 90:11613–11617.
- Arulananandam, A. R. N., A. Kister, M. J. McGregor, D. F. Wyss, G. Wagner, and E. L. Reinherz. 1994. Interaction between human CD2 and CD58 involves the major β sheet surface of each of their respective adhesion domains. *J. Exp. Med.* 180:1861–1871.
- Bodian, D. L., E. Y. Jones, K. Harlos, D. I. Stuart, and S. J. Davis. 1994. Crystal structure of the extracellular region of the human cell adhesion molecule CD2 at 2.5 Å resolution. *Structure.* 2:755–766.
- Bork, P., L. Holm, and C. Sander. 1994. The immunoglobulin fold. *J. Mol. Biol.* 242:309–320.
- Carl, P., C. H. Kwok, G. Manderson, D. W. Speicher, and D. E. Discher. 2001. Forced unfolding modulated by disulfide bonds in the Ig domains of a cell adhesion molecule. *Proc. Natl. Acad. Sci. USA.* 98:1565–1570.
- Chilkoti, A., T. Boland, B. D. Ratner, and P. S. Stayton. 1995. The relationship between ligand-binding thermodynamics and protein-ligand interaction forces measured by atomic force microscopy. *Biophys. J.* 69:2125–2130.
- Chothia, C., and E. Y. Jones. 1997. The molecular structure of cell adhesion molecules. *Annu. Rev. Biochem.* 66:823–862.
- Davis, S. J., S. Ikemizu, M. K. Wild, and P. A. van der Merwe. 1998a. CD2 and the nature of protein interactions mediating cell-cell recognition. *Immunol. Rev.* 163:217–236.

- Davis, S. J., E. A. Davies, M. G. Tucknott, E. Y. Jones, and P. A. van der Merwe. 1998b. The role of charged residues mediating low affinity protein-protein recognition at the cell surface by CD2. *Proc. Natl. Acad. Sci. USA.* 95:5490–5494.
- Evans, E., and K. Ritchie. 1997. Dynamic strength of molecular adhesion bonds. *Biophys. J.* 72:1541–1555.
- Evans, E. 1998. Energy landscapes of biomolecular adhesion and receptor anchoring at interfaces explored with dynamic force spectroscopy. *Faraday Discuss.* 111:1–16.
- Fisher, T. E., M. Carrion-Vazquez, A. F. Oberhauser, H. Li, P. E. Marszalek, and J. M. Fernandez. 2000. Single molecule force spectroscopy of modular proteins in the nervous system. *Neuron.* 27:435–446.
- Humphrey, W., A. Dalke, and K. Schulten. 1996. VMD—visual molecular dynamics. *J. Mol. Graph.* 14:33–38.
- Ikemizu, S., L. M. Sparks, P. A. van der Merwe, K. Harlos, D. I. Stuart, E. Y. Jones, and S. J. Davis. 1999. Crystal structure of the CD2-binding domain of CD58 (lymphocyte function-associated antigen 3) at 1.8 Å. *Proc. Natl. Acad. Sci. USA.* 96:4289–4294.
- Isralewitz, B., M. Gao, and K. Schulten. 2001. Steered molecular dynamics and mechanical functions of proteins. *Curr. Opin. Struct. Biol.* 11:224–230.
- Izrailev, S., S. Stepaniants, M. Balsera, Y. Oono, and K. Schulten. 1997. Molecular dynamics study of unbinding of the Avidin-biotin complex. *Biophys. J.* 72:1568–1581.
- Kale, L. V., R. D. Skeel, M. Bhandarkar, R. Brunner, A. Gurse, N. Krawetz, J. Phillips, A. Shinazaki, K. Varadarajan, and K. Schulten. 1999. NAMD2: greater scalability for parallel molecular dynamics. *J. Comp. Phys.* 151:283–312.
- Kim, M., Z. J. Sun, O. Byron, G. Campbell, G. Wagner, J. Wang, and E. L. Reinherz. 2001. Molecular dissection of the CD2–CD58 counter-receptor interface. *J. Mol. Biol.* 312:711–720.
- Koyasu, S., T. Lawton, D. Novick, M. A. Recny, R. F. Siliciano, B. P. Wallner, and E. L. Reinherz. 1990. Role of interaction of CD2 molecules with lymphocyte function-associated antigen 3 in T-cell recognition of nominal antigen. *Proc. Natl. Acad. Sci. USA.* 87:2603–2607.
- Krammer, A., H. Liu, B. Isralewitz, V. Vogel, and K. Schulten. 1999. Forced unfolding of the fibronectin type III module reveals a tensile molecular recognition switch. *Proc. Natl. Acad. Sci. USA.* 96:1351–1356.
- Lu, H., B. Isralewitz, A. Krammer, V. Vogel, and K. Schulten. 1998. Unfolding of titin immunoglobulin domains by steered molecular dynamics simulation. *Biophys. J.* 75:662–671.
- MacKerell, A. D., D. Bashford, M. Bellot, R. L. Dunbrack, Jr., J. Evansec, M. J. Field, S. Fisher, J. Gao, H. Guo, S. Ha, D. Joseph, L. Kuchnir, K. Kuczera, F. T. K. Lau, C. Mattos, S. Michnick, T. Ngo, D. T. Nguyen, B. Prodhom, I. W. E. Reiher, B. Roux, M. Schlenkrich, J. Smith, R. Stote, J. Straub, M. Watanabe, J. Wiorkiewicz-Kuczera, D. Yin, and M. Karplus. 1998. All-hydrogen empirical potential for molecular modeling and dynamics studies of proteins using the CHARMM22 force field. *J. Phys. Chem. B.* 102:3586–3616.
- Marszalek, P. E., H. Lu, H. B. Li, M. Carrion-Vazquez, A. F. Oberhauser, K. Schulten, and J. M. Fernandez. 1999. Mechanical unfolding intermediates in titin modules. *Nature.* 402: 100–103.
- Moigneon, P., H. Chang, B. P. Wallner, C. Stebbins, A. Z. Frey, and E. L. Reinherz. 1989. CD2-mediated adhesion facilitates T lymphocyte antigen recognition function. *Nature (Lond.).* 339:312–314.
- Wang, J., A. Smolyar, K. Tan, J. Liu, M. Kim, Z. J. Sun, G. Wagner, and E. L. Reinherz. 1999. Structure of a heterophilic adhesion complex between the human CD2 and CD58 (LFA-3) counterreceptors. *Cell.* 97:791–803.
- Zhu, B., E. A. Davies, P. A. van der Merwe, T. Calvert, and D. E. Leckband. 2002. Direct measurements of heterotypic adhesion between the cell surface proteins CD2 and CD48. *Biochemistry.* 41:12163–12170.